1

Utility of *Galleria mellonella* larvae for evaluating nanoparticle toxicology

3

Laura Moya-Andérico[1], Marija Vukomanovic[2], Maria del Mar Cendra[1], Miriam Segura-Feliu[3,4,5,6], Vanessa Gil[3,4,5,6], José A. del Río[3,4,5,6], Eduard Torrents[1,7]*

6

[1]Bacterial Infections: Antimicrobial Therapies group, Institute for Bioengineering of Catalonia (IBEC), The Barcelona Institute of Science and Technology (BIST), Barcelona, Spain.

[2]Advanced Materials Department, Jozef Stefan Institute, Ljubljana, Slovenia.

[3]Molecular and Cellular Neurobiotechnology, Institute for Bioengineering of Catalonia (IBEC), The Barcelona Institute of Science and Technology (BIST), Barcelona, Spain.

[4]Centro de Investigación Biomédica en Red sobre Enfermedades Neurodegenerativas (CIBERNED), Madrid, Spain.

[5]Department of Cell Biology, Physiology and Immunology, Universitat de Barcelona, Barcelona, Spain.

[6]Institute of Neurosciences, Universitat de Barcelona, Barcelona, Spain.

[7]Microbiology Section, Department of Genetics, Microbiology, and Statistics, Biology Faculty, Universitat de Barcelona, Barcelona, Spain.

19

*Corresponding author: Eduard Torrents (etorrents@ibecbarcelona.eu). Bacterial Infections: Antimicrobial Therapies group, Institute for Bioengineering of Catalonia (IBEC), The Barcelona Institute of Science and Technology (BIST), Barcelona, Spain. Phone: +34 93 403756.

24

25

26 **Abstract**

27   The use of nanoparticles in consumer products is currently on the rise, so it is important

28 to have reliable methods to predict any associated toxicity effects. Traditional *in vitro* assays

29 fail to mimic true physiological responses of living organisms against nanoparticles whereas

30 murine *in vivo* models are costly and ethically controversial. For these reasons, this study aimed

31 to evaluate the efficacy of *Galleria mellonella* as an alternative, non-rodent *in vivo* model for

32 examining nanoparticle toxicity. Silver, selenium, and functionalized gold nanoparticles were

33 synthesized, and their toxicity was assessed in *G. mellonella* larvae. The degree of acute toxicity

34 effects caused by each type of NP was efficiently detected by an array of indicators within the

35 larvae: LD_{50} calculation, hemocyte proliferation, NP distribution, behavioral changes, and

36 histological alterations. *G. mellonella* larvae are proposed as a nanotoxicological model that

37 can be used as a bridge between *in vitro* and *in vivo* murine assays in order to obtain better

38 predictions of NP toxicity.

39

40 **Keywords:** *Galleria mellonella*, nanoparticles, nanotoxicity, non-rodent *in vivo* model, toxicity

41 screening, hemocytes

42

43 **Running title:** *Galleria mellonella* as a nanotoxicological *in vivo* model

44

1. Introduction

In recent years, nanoparticles (NPs) have become the target of numerous studies as they have shown promising potential in a wide range of human applications. Their unique physicochemical properties such as nanosize, solubility, surface area, and surface chemistry, among others, deem nanoparticles as an attractive technology in many industrial and biomedical fields (Bouwmeester et al., 2014). Popular elements like silver, gold, and selenium have been used as nanomaterials due to their known beneficial properties. Silver nanoparticles (AgNPs) are commonly used in a variety of consumer products such as cosmetics, textiles, home appliances, and medical devices and treatments (Ahamed et al., 2010; Schluesener and Schluesener, 2013; Vance et al., 2015) due to the renowned antimicrobial properties of silver (Mijnendonckx et al., 2013; Schluesener and Schluesener, 2013). Gold nanoparticles (AuNPs) have been used as a treatment for rheumatoid arthritis as well as in cancer therapy, drug delivery, and biosensors, among other uses (Finkelstein et al., 1976; Alkilany and Murphy, 2010; Zhang et al., 2010). Selenium nanoparticles (SeNPs) have also been used extensively in cancer therapy studies due to the potential anti-carcinogenic activity of selenium compounds. Selenium also provides several health benefits as it has been shown to improve immune, cognitive, and reproductive functions (Rayman, 2012; Fernandes and Gandin, 2015; Evans et al., 2017). Despite their plethora of applications, the use of nanoparticles has exhibited certain toxic effects, so it is critical to obtain a better understanding of their potential adverse effects on humans and the environment.

AgNPs have been reported to produce several toxic effects. Previous *in vitro* studies have shown that these nanoparticles can commonly induce oxidative stress due to the generation of reactive oxygen species (ROS) within the cells which can lead to DNA damage and apoptotic cell death (Hsin et al., 2008; Kim et al., 2009b; Chairuangkitti et al., 2013; Rinna et al., 2015). Furthermore, *in vivo* studies also showed increased ROS levels and revealed that AgNPs may

70 also cause toxic effects in main organs such as brain, lung, liver, kidney, spleen, and intestine

71 as well as in the nervous and immune systems. Besides the route of administration, the cytotoxic

72 and genotoxic effects of AgNPs are also dependent on the size, dose, and coating of the

73 nanoparticles (Tang et al., 2009; Kim et al., 2010; Xue et al., 2012; De Jong et al., 2013;

74 Recordati et al., 2016; Shrivastava et al., 2016; Souza et al., 2016). AuNPs have also displayed

75 the capability to induce oxidative stress generated by the production of nitric oxide which

76 oxidizes DNA, proteins, and lipids followed by potential cell necrosis or apoptosis. The toxic

77 effects are size-dependent with smaller nanoparticles having the most distribution throughout

78 body organs and mainly target the liver and spleen (De Jong et al., 2008; Chen et al., 2009; Jia

79 et al., 2009; Shrivastava et al., 2016). The effects also depend on whether the nanoparticles are

80 functionalized or not. Metallic gold is considered biologically safe while functionalized AuNPs

81 have reported higher cytotoxic effects (Goodman et al., 2004; Zhang et al., 2010). On the other

82 hand, functionalization enhances the stability of the nanoparticles and can facilitate targeted

83 drug delivery (Khoshnevisan et al., 2018). The toxicity of selenium compounds is greatly

84 dependent on the concentration of selenium administered as high levels have been reported to

85 be toxic as well as mutagenic and carcinogenic. The chemical form of selenium also plays a

86 role in toxicity with inorganic forms like sodium selenite being more genotoxic when compared

87 to organic forms like methyl-selenocysteine. Other toxic effects include selenosis, production

88 of oxidative stress, induction of DNA damage, and interference in endocrine function and

89 hormone synthesis (Yan and Spallholz, 1993; Bronzetti et al., 2001; Letavayova et al., 2008;

90 Valdiglesias et al., 2010). The majority of these toxic effects were found *in vitro* while few

91 toxicity studies have been done *in vivo*. One study tested selenium concentrations commonly

92 used in the poultry industry in broiler chickens, and it found that selenium concentrated mainly

93 in the spleen with no histopathological damage seen in any of the tissues tested (Gangadoo et

94   al., 2020). Other *in vivo* studies mainly focus on selenium effects on cellular and neurological

95   functions combined with organism mortality (Rohn et al., 2018).

96   The majority of NP toxicity data is usually obtained with *in vitro* assays. Instead, it

97   should be generated with *in vivo* models that replicate the true physiological responses of living

98   organisms to nanomaterials. (Valdiglesias et al., 2010; Barile, 2013). The use of mammals for

99   toxicological testing is expensive, time-consuming, and ethically controversial so alternative

100   models need to be used. For this reason, non-mammalian animal models such as *Danio rerio*,

101   *Drosophila melanogaster*, and *Caenorhabditis elegans* are commonly used in the laboratory

102   for toxicological screenings (Leung et al., 2008; Ahamed et al., 2010; Rand et al., 2014).

103   Another invertebrate that has been gaining popularity as an *in vivo* model is *Galleria mellonella*

104   (greater wax moth). When compared to other *in vivo* models, the larval stage of *G. mellonella*

105   has many attractive advantages: convenient size for manipulation, inexpensive to purchase and

106   breed, does not require much space or special infrastructure, low biohazard risk, and are more

107   ethically accepted. Larvae used for testing are about 2 cm in length and weigh about 200 mg

108   which facilitates the administration of the precise dose of nanomaterials by injection. Unlike

109   other alternative models, the larvae can survive at 37°C which allows for the study of

110   nanomaterials at the same temperature of the human body (Desbois and Coote, 2012; Junqueira,

111   2012; Champion et al., 2016). Furthermore, the immune system of the larvae closely resembles

112   the innate immune response of mammals (Browne et al., 2013; Wojda, 2017). *G. mellonella*

113   has been used to evaluate the behavior, efficacy, and toxicity of antimicrobial compounds, and

114   the results obtained have been proven useful for predicting human response to antibiotics

115   (Thomas et al., 2013; Ignasiak and Maxwell, 2017). The model has also been used to test the

116   toxicity of ionic liquids and food preservatives as well as many other compounds (Megaw et

117   al., 2015; Dolan et al., 2016; Maguire et al., 2016; Allegra et al., 2018).

118   The aim of this study was to test the potential of *G. mellonella* as an *in vivo* model for

119   the study of specific nanoparticles in order to provide a simple, economical, and robust toxicity

120   model for the nanomedicine field.

121

122   **2. Materials and methods**

123   ***2.1. Nanoparticle (NP) synthesis and characterization***

124   Silver nanoparticles (AgNPs) were synthesized using silver nitrate precursor (AgNO$_3$,

125   0.8 mg/ml, 50 ml) which was pre-heated to 100ºC. Instant addition of sodium borohydride (0.2

126   mg/ml, 10 ml) into the boiling precursor resulted in a color change from transparent to yellow

127   or brown indicating finalization of the reaction.

128   Selenium nanoparticles (SeNPs) were synthesized using sodium selenite precursor

129   (Na$_2$SeO$_3$, 0.8 mg/ml, 50 ml). The NPs formation took place slowly and in the following two

130   hours, a color change from transparent to intense orange indicated the end of the reaction.

131   Mixing was continued overnight at room temperature to ensure NPs stabilization and

132   agglomeration prevention.

133   Gold nanoparticles (AuNPs) were synthesized in the presence of amino acids which

134   functionalized their surface to grant antimicrobial properties (Vukomanović et al., 2014). This

135   way, increased toxicity by functionalization will be assayed. Since apatite is not toxic and can

136   be used to stabilize AuNPs, it was used as a template and was synthesized using homogeneous

137   sonochemical precipitation (Jevtić et al., 2008). The template was dispersed by 10-minute

138   sonication in water containing 1 ml of isopropanol (amplitude 80%, on:off cycles 0.2:01s; VCX

139   750, Sonics®, Newtown, CT, USA). Chloroauric acid (HAuCl$_4$, 0.8 mg/ml, 50 ml), used as a

140   gold precursor, was added to pre-sonicated apatite template (1.5 mg/ml, 50 ml). Upon addition

141   of amino acid solutions containing histidine, arginine, and lysine amino acids (HAL) (0.15

142   mg/ml for each amino acid), the sonication was continued for an additional 30 minutes. The

143 reaction was finished when the yellow-colored precursor turned violet indicating NPs

144 formation.

145   All the NPs were centrifuged at 2500 x g for 20 minutes to separate the supernatant, re-

146 dispersed in 20 ml of water, and frozen on dry ice. After 24 hours at -80ºC, they were freeze-

147 dried.

148   For morphological and structural characteristics, NPs were sonochemically dispersed in

149 water, deposited on copper grids, and observed using a transmission electron microscope

150 (TEM, Tecnai^{TM} Spirit 120kV, FEI^{TM}, Hillsboro, OR, USA). The zeta potential measurements

151 were performed using a Nanosizer (Malvern Panalytical, Malvern, UK).

152

153   ***2.2. Cell culture and nanoparticle in vitro toxicity***

154   The toxicity of the different nanoparticles was assessed in the adenocarcinomic lung

155 epithelial cell line A549 (ATCC® CCL-185). Cells were cultured in a 96-well polystyrene plate

156 and grown in Dulbecco's Modified Eagle Medium (complete DMEM): Nutrient mixture F12

157 (DMEM/F12; Thermo Fisher Scientific, Madrid, Spain) supplemented with 10% (v/v)

158 decomplemented fetal bovine serum (dFBS), 100 Units/ml penicillin, and 100 Units/ml

159 streptomycin (Thermo Fisher Scientific, Madrid, Spain). Cells were maintained in a humidified

160 incubator at 37ºC and 5% (v/v) CO_2 (ICOmed, Memmert, Schwabach, Germany). On the other

161 hand, Au(HAL)NPs, AgNPs, and SeNPs were dispersed in complete DMEM by ultrasonication

162 (amplitude: 18%, W= 250W, on:off= 2:1s for 30s; Digital Sonifier® 250, Branson Ultrasonics,

163 Danbury, CT, USA). Dispersed NPs were subsequently adjusted in 200 µl of complete DMEM

164 to be tested, in triplicates, at the concentrations of 0, 0.001, 0.005, 0.01, 0.05, 0.1, 0.15, 0.2,

165 0.5, 1.0 and 2.0 mg/ml in the A549 cells. Cell incubation with 1:10 dilution of dimethyl

166 sulfoxide (DMSO) was used as a positive control for toxicity. After 24-hour incubation, cellular

167 toxicity was determined using the PrestoBlue^{TM} Cell Viability Reagent (Invitrogen, Carlsbad,

168   CA, USA) following the manufacturers' instructions. Briefly, 20 µl of PrestoBlue[TM] was added

169   to each well and the plate was subsequently incubated for 1 h at 37ºC. After incubation,

170   absorbance was read at λ=570 using a microplate reader (Infinite[®] M200 Microplate reader,

171   Tecan, Männedorf, Switzerland), and the given values were corrected by the

172   respective absorbance at λ=600, as recommended by the manufacturer. Greater metabolic

173   activity of the cells (live cells) correlates to higher absorbance values.

174   Cell toxicity was determined using the absorbance values of the untreated cells

175   ($Abs_{570}/Abs_{600} \sim 44532$) as 100% cell viability. The concentration of each NP that caused 50%

176   of cell toxicity (cytotoxicity 50%; CC_{50}) was calculated using Prism 8.0 (GraphPad Software,

177   San Diego, CA, USA).

178

179   *2.3. G. mellonella growth and maintenance*

180   *G. mellonella* larvae were reared at 34ºC and fed an artificial diet consisting of corn

181   flour, wheat flour, skim milk powder, cereals, dried brewer's yeast, honey, and glycerol as

182   previously described (Moya-Anderico et al., 2020). Prior to inoculation, last instar larvae were

183   incubated without food at 15°C for a maximum period of 24 hours (Ramarao et al., 2012).

184

185   *2.4. G. mellonella in vivo nanoparticle toxicity*

186   Groups of 5 larvae (200-250 mg each) were injected with a 22-gauge syringe (Hamilton,

187   Reno, NV, USA) through the top right proleg using a 10 µl inoculum of various nanoparticle

188   concentrations. The control group was inoculated with 10 µl of 1x PBS (Fisher Scientific,

189   Madrid, Spain) in the same manner. After inoculation, the larvae were kept at 37ºC for 37-72

190   hours with larval mortality observations done at 3, 16, 24, 37, 48, and 72 hours post-injection.

191   Survival curves were plotted using Kaplan-Meier analysis and statistically significant

192   differences were determined by the log-rank test (Prism 8.0, GraphPad Software, San Diego,

193 CA, USA). The median lethal dose (LD_{50}) was determined as the nanoparticle concentration

194 required to kill 50% of the larvae in 48 hours (Prism 8.0, GraphPad Software, San Diego, CA,

195 USA).

196

197 ### *2.5. G. mellonella hemocyte proliferation*

198 To measure hemocyte proliferation, the hemolymph was extracted from the larvae by

199 cutting the tail off with a sterile surgical blade (size 23, Paramount Surgimed, New Delhi, India)

200 and allowing the hemolymph to drain out into an Eppendorf tube for 10 minutes on ice. The

201 hemolymph was centrifuged at 4ºC for 5 minutes at 1000 x *g* to isolate hemocytes. The

202 supernatant was removed and the hemocytes were washed once with PBS 1x. The washed cells

203 were resuspended in PBS 1x, diluted 1:2 with trypan blue (Sigma-Aldrich, Lyon, France), and

204 loaded onto a Neubauer counting chamber (Blaubrand®, Brand®, Wertheim, Germany) to

205 determine hemocyte count.

206

207 ### *2.6. Nanoparticle distribution and microscopy studies*

208 *G. mellonella* larvae were injected with 250 mg/kg body weight of AgNPs and 1250

209 mg/kg body weight of Au(HAL)NPs and 20 hours later, hemocytes were extracted and stained

210 with FM™ 4-64 dye (Thermo Fisher Scientific, Madrid, Spain) according to the manufacturer's

211 specifications. The hemocytes were then imaged using a confocal laser scanning microscope

212 (LSM 800, Zeiss, Jena, Germany) and nanoparticles were visualized by light reflection using

213 the 640 nm laser and the 40x/1.3 oil objective. All microscopy images were analyzed with

214 ImageJ FIJI (National Institutes of Health, Bethesda, MD, USA).

215 For NP distribution, larvae were injected with different concentrations of NPs and after

216 37 hours (for SeNPs) and 72 hours (for Au(HAL) and Ag nanoparticles), the larvae were

217 imaged to monitor nanoparticle accumulations within the body using an inverted fluorescent

218 microscope (ECLIPSE Ti-S/L100, Nikon, Tokyo, Japan) connected to a DS-Qi2 camera

219 (Nikon, Tokyo, Japan).

220

221 *2.7. Behavioral tracking studies*

222 10 µl of nanoparticles were injected into three larvae per group at a final concentration

223 of 2841 mg/kg body weight of Au(HAL)NPs, 2841 mg/kg body weight of AgNPs, and 114

224 mg/kg body weight of SeNPs. As a control, two larvae were injected with 10 µl of PBS. About

225 1 hour after inoculation, two or three larvae were deposited in the center of a 150 mm diameter

226 plastic petri dish which was then placed on a homemade transilluminator. Larval movement

227 was monitored for about 73 seconds using a USB twain supported camera (C270, Logitech,

228 Lausanne, Switzerland) and the OPTIKA Vision Pro video time-lapse software (100 ms/frame

229 at 640 x 360 dpi; OPTIKA, Ponteranica, Italy). Images were then compiled as single image

230 stacks and exported as uncompressed AVI video files. The resulting paths were analyzed using

231 the MTrack2 plug-in of the ImageJ software (National Institutes of Health, Bethesda, MD,

232 USA) and the data was analyzed by determining statistically significant differences with an

233 unpaired *t*-test (Prism 8.0, GraphPad Software, San Diego, CA, USA).

234

235 *2.8. Histological analysis*

236 The same larvae used in the tracking studies were subsequently used for the histological

237 analysis. In order to avoid excessive body bending during processing, larvae were fixed and

238 dehydrated inside 1 cm diameter glass tubes. Thus, larvae were fixed in 1% phosphate-buffered

239 paraformaldehyde (pH 7.3) overnight at 4ºC. After rinsing in PBS 1x, samples were dehydrated

240 with increasing concentrations of ethanol (70, 90, and 96%), cleared in butanol, and embedded

241 in low melting paraffin (56-58ºC, Lab-o-wax, Histo-line Laboratories, Pantigliate, Italy).

242 Paraffin blocks were sectioned at 10 μm on a standard rotary microtome (Leica, Wetzlar,

10

243　Germany). These sections were collected on gelatinized slides and then stained by hematoxylin

244　eosin (HE) following standard protocols. The stained sections were mounted in Eukitt® and

245　examined microscopically in an optical microscope (BX61, Olympus®, Tokyo, Japan) equipped

246　with a DP12 digital camera (Olympus®, Tokyo, Japan). Low magnification images were

247　obtained using an MPlan Apo 1.24/0.04 objective (Olympus®, Tokyo, Japan).

248

249　**3.　Results**

250　*3.1. NP characterization*

251　The nanoparticles to be used as nano-toxicity models, AgNPs, Au(HAL)NPs, and

252　SeNPs, were characterized by a negative net surface charge with very similar surface charge

253　magnitudes (-17 mV, -14 mV, and -16 mV, respectively) (Fig. 1). Morphologically, all of them

254　have a spherical shape with a very narrow size distribution. AgNPs are small spheres with 12

255　nm diameter which were detected as small and large clusters with an average size of 60 nm and

256　306 nm, respectively. The Au(HAL)NPs are 15 nm-sized particles coated by an organic layer

257　and deposited to the surface of apatite plates. The average size of these structures is 76 nm and

258　194 nm. In the case of SeNPs, they are small particles with a size of 9 nm and very stable. They

259　were detected as individual NPs as well as in clusters with 36 nm in size.
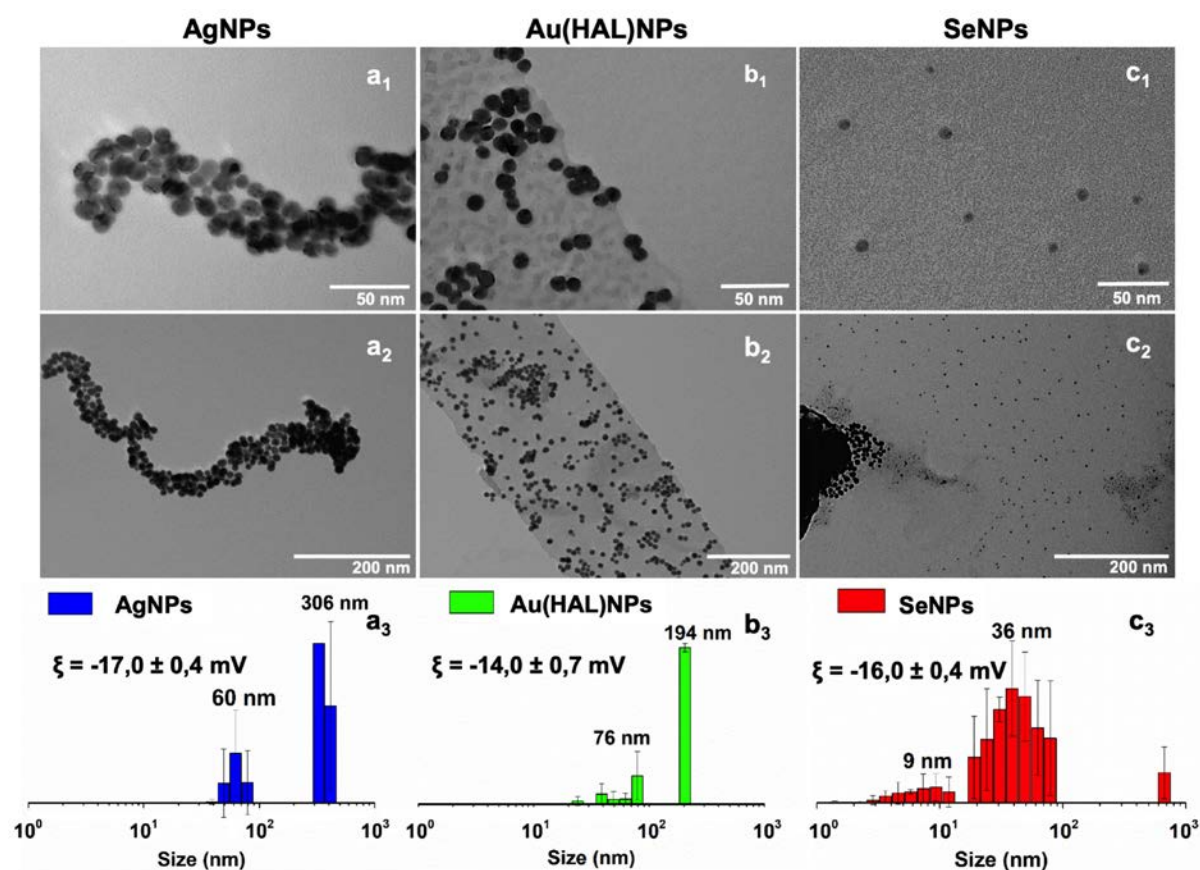
Fig. 1. Morphology, size distribution, and zeta potential of **(a)** Ag, **(b)** Au(HAL), and **(c)** Se nanoparticles used for the toxicological study. Synthesized nanoparticles were characterized using TEM and Nanosizer techniques.

260

261 ### 3.2. In vitro nanoparticle toxicity

262   The toxicity of all NPs was first studied *in vitro* using A549 cells. Cells incubated

263 without any treatment resulted in 100% survival while the DMSO-exposed cells remained blue

264 after the addition of PrestoBlue[TM] which indicated cell death. As the concentrations of NPs

265 tested increased, cell survival decreased. The Au(HAL)NPs were the least cytotoxic with a

266 CC_{50} of 1.018 mg/ml. SeNPs and AgNPs were more cytotoxic with a CC_{50} of 0.163 mg/ml and

267 0.190 mg/ml, respectively. The CC_{50} of similar NPs tested in macrophages were gathered from

268 the literature (see Table 1) and compared against the CC_{50} values in A549 cells. The AgNPs

269 and SeNPs were more toxic to macrophages than to A549 cells while the toxicity of

270 Au(HAL)NPs was in a similar range for both types of cells.

	In vitro - CC$_{50}$ (mg/ml)		In vivo - LD$_{50}$ (mg/kg)	
	A549	**Macrophages**	*G. mellonella*	**Murine models**
Au(HAL)NPs	1.018	> 0.1* (Zhang et al., 2011; Hashimoto et al., 2015)	2023	> 1000* (Sonavane et al., 2008; Kim et al., 2009a)
AgNPs	0.190	0.008-0.0384 (Pratsinis et al., 2013; Arai et al., 2015; Mannerström et al., 2016; Makama et al., 2018)	939	> 60 (Xue et al., 2012; Zhang et al., 2013; Pinzaru et al., 2018)
SeNPs	0.163	< 0.01 (Yazhiniprabha and Vaseeharan, 2019)	89	> 2.5 (Ren et al., 2019; Shahabi et al., 2019)

271 **Table 1.** Comparison of toxicity values obtained in both *in vitro* and *in vivo* studies. CC$_{50}$ and LD$_{50}$ values in gray
272 columns (macrophages and murine models) were obtained from the literature while CC$_{50}$ and LD$_{50}$ values in white
273 columns (A549 and *G. mellonella*) were gathered from this study. Asterisk (*) refers to values obtained with non-
274 functionalized AuNPs.

275 ### 3.3. In vivo nanoparticle toxicity and hemocyte proliferation

276 Different concentrations of Au(HAL), Ag, and Se nanoparticles were injected into *G.*
277 *mellonella* larvae to study their toxicity *in vivo*. The LD$_{50}$ was calculated and it was found that
278 the NPs exhibit different levels of toxicity (Fig. 2). Au(HAL)NPs were the least toxic with an
279 LD$_{50}$ of 2023 mg/kg while AgNPs and SeNPs yielded much lower LD$_{50}$ values (939 mg/kg and
280 89 mg/kg, respectively) thus demonstrating their high toxicity to the larvae, especially the
281 SeNPs. All LD$_{50}$ values obtained were compared to LD$_{50}$ values acquired with murine models
282 which were compiled from the literature (Table 1). The LD$_{50}$ values obtained with
283 Au(HAL)NPs, AgNPs, and SeNPs in *G. mellonella* were higher than those acquired with
284 murine models.
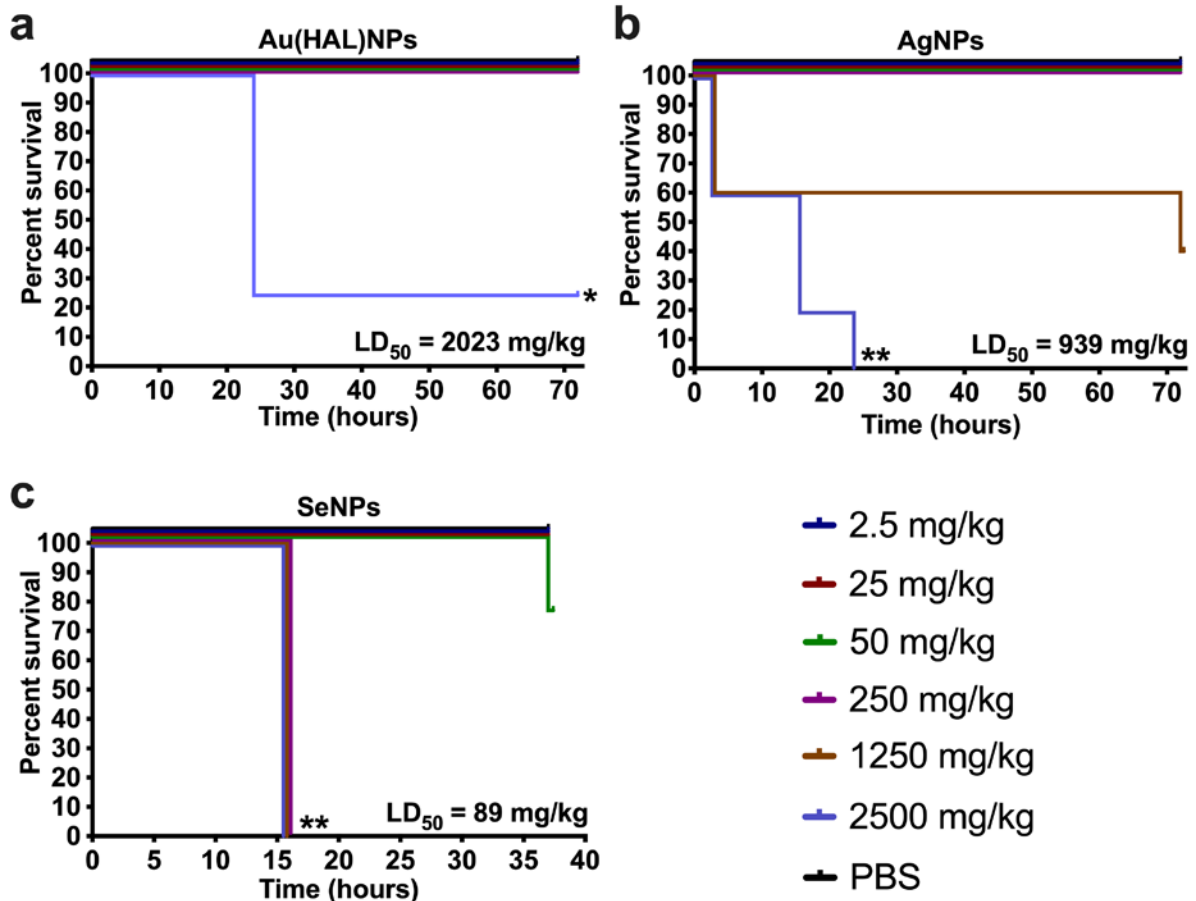
Fig. 2. Kaplan-Meier survival curve of *G. mellonella* larvae injected with various concentrations of **(a)** Au(HAL), **(b)** Ag, and **(c)** Se nanoparticles. As a control, larvae were injected with only PBS. Larval mortality was monitored for 37-72 hours post-injection with observations done at 3, 16, 24, 37, 48, and 72 hours post-injection. Asterisks: statistically significant difference versus PBS control in a log-rank test (*: p-value <0.05; **: p-value <0.01). The results presented in this figure are representative of the same experiment that was repeated several times, and it yielded identical results every time.

285

286   Nanoparticles are often recognized as foreign materials that can trigger various innate

287   immune responses (Jones and Grainger, 2009). The activation of the innate immune system in

288   *G. mellonella* can cause changes in the number of circulating hemocytes (Browne et al., 2013).

289   For this reason, hemocyte levels were monitored in all larval test groups. All NP concentrations

290   produced an increase in the number of hemocytes present in the larvae when compared to the

291   PBS control group (Fig. 3). However, hemocyte proliferation did not rise with the ascending

292   nanoparticle concentrations as it was expected. For Au(HAL)NPs, hemocyte proliferation was

293   highest (3.6×10^6 cells/ml) with the lowest concentration (50 mg/kg) and the values descended

as the NP concentrations increased (Fig. 3a). For AgNPs, the two highest hemocyte

proliferation values (2.6×10^6 and 3.1×10^6 cells/ml) were obtained with the two lowest

concentrations (50 and 250 mg/kg, respectively) (Fig. 3b). On the other hand, the hemocyte

values did not change much among the different concentrations of SeNPs (Fig. 3c).
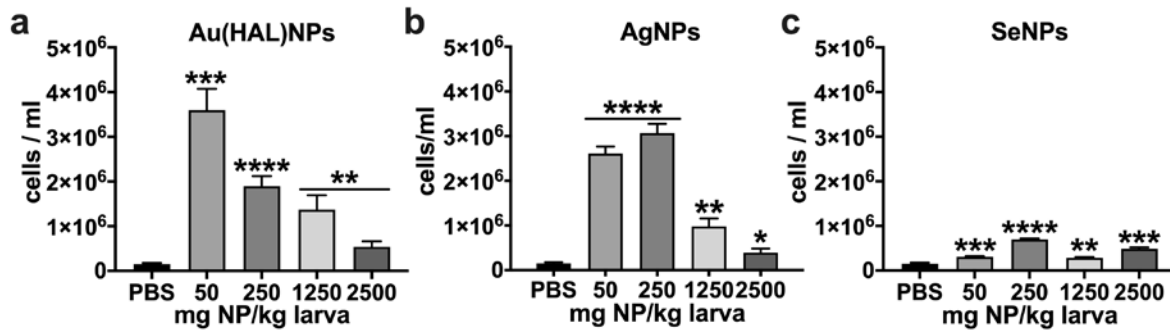
Fig. 3. Effect of **(a)** Au(HAL), **(b)** Ag, and **(c)** Se nanoparticles on hemocyte density in *G. mellonella*. Hemocytes were counted at 72 hours post-injection for Au(HAL)NPs and AgNPs and at 37 hours post-injection for SeNPs. As a control, hemocytes from larvae injected with only PBS were also counted. Asterisks: statistically significant difference versus PBS control in an unpaired *t*-test (*: *p*-value <0.05; **: *p*-value <0.01; ***: *p*-value <0.001; ****: *p*-value <0.0001).

3.4. In vivo nanoparticle distribution

To determine whether the nanoparticles triggered hemocyte-driven internalization, hemocytes were isolated from larvae that were injected with 1250 mg/kg body weight of Au(HAL)NPs and 250 mg/kg body weight of AgNPs and then imaged under a confocal microscope. These concentrations were chosen as they were the concentrations prior to the corresponding LD_{50}. Using light reflection, aggregates of nanoparticles (depicted in cyan) could be observed inside the hemocytes as pointed by the white arrows in Fig. 4. As it can be distinctly observed in the orthogonal views, a single hemocyte was able to internalize more than one nanoparticle simultaneously.
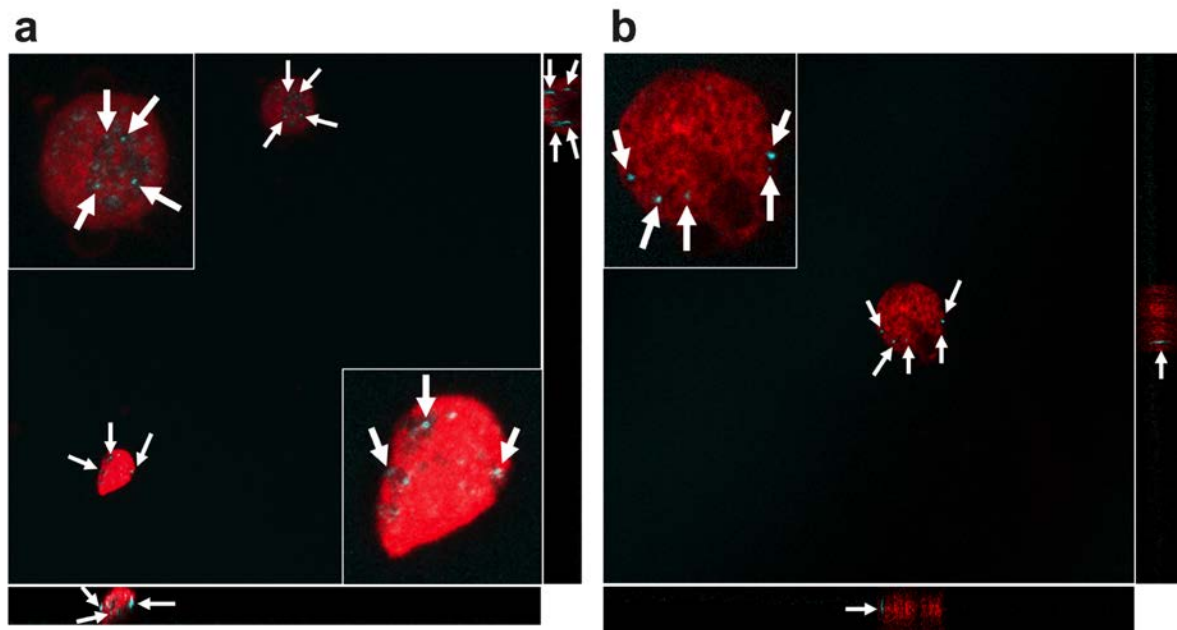
Fig. 4. Confocal laser scanning microscope images of *G. mellonella* hemocytes stained with FM™ 4-64 dye. Larvae were injected with **(a)** 1250 mg/kg body weight of Au(HAL)NPs and with **(b)** 250 mg/kg body weight of AgNPs followed by hemocyte extraction 20 hours later. Center images are the sum of all stack images and the orthogonal views are seen to the side and underneath. The membrane of the hemocytes stained red while aggregates of NPs were visualized using light reflection and shown in cyan while pointed at by white arrows.

312

313   The NPs were not only found within hemocytes, but they were also present in the body

314 of the larvae with the majority being accumulated in the caudal area (tails) (Fig. 5). Other NP

315 accumulations throughout the rest of the larval body were not clearly seen (Fig. 5a). This event

316 was still seen when the movement of the larvae was partially or fully restricted. To check

317 whether NP accumulation in the tails was due to the peristaltic movement, larvae were injected

318 with 250 mg/kg body weight and 1250 mg/kg body weight of AgNPs and Au(HAL)NPs,

319 respectively. Then, the larvae were kept in three different conditions: without movement

320 (cooled at 15°C), with limited movement (inside Eppendorf tubes), and without restricted

321 movement (free inside petri dishes). In all three conditions, the NPs accumulated towards the

322 caudal part of the larvae with the majority concentrating in the tails (Fig. 5b).

16
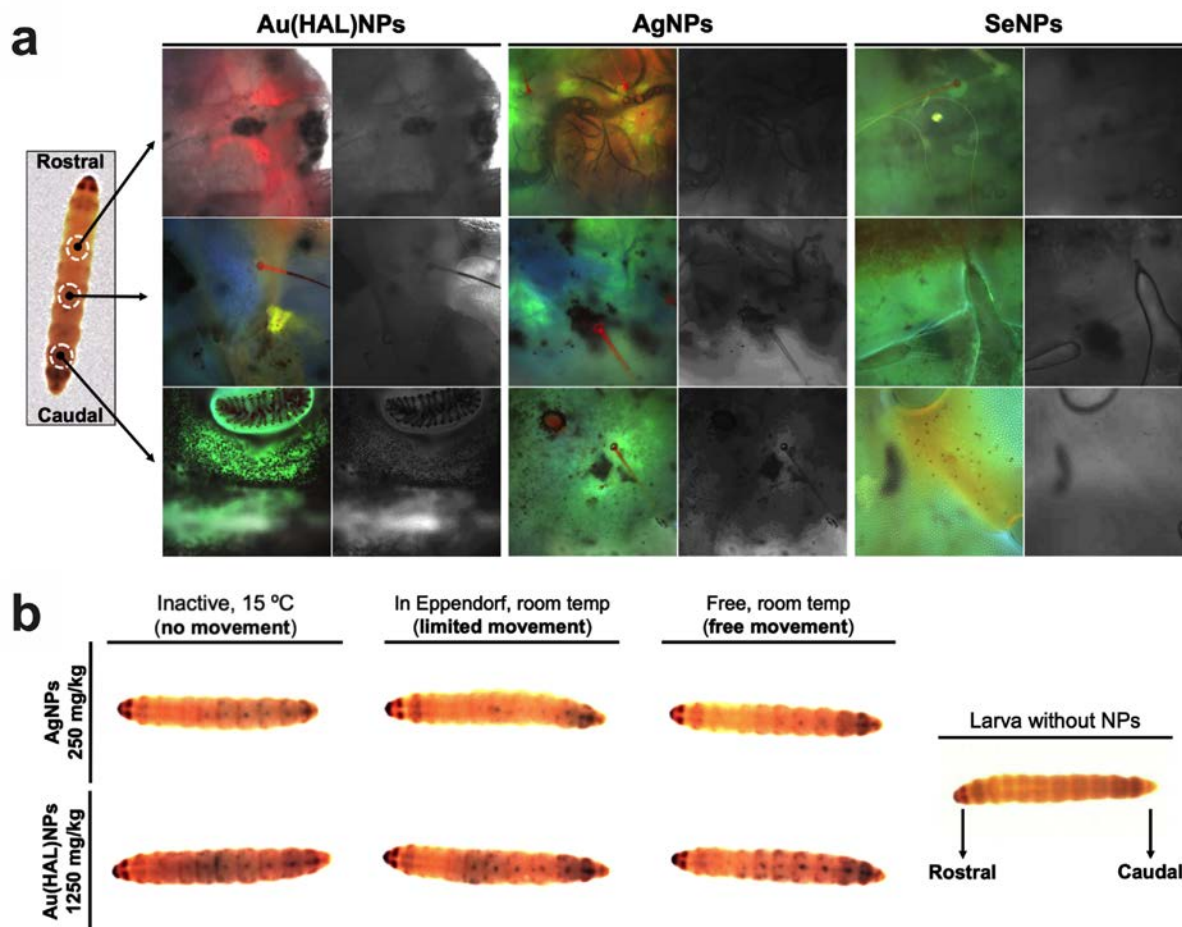
Fig. 5. Distribution of Au(HAL), Ag, and Se nanoparticles throughout the body of *G. mellonella* larvae. **(a)** To determine NP accumulations, larvae were imaged with a fluorescent microscope at 72 hours post-injection for Au(HAL) and Ag nanoparticles and at 37 hours post-injection for SeNPs. **(b)** 250 mg/kg body weight of AgNPs and 1250 mg/kg body weight of Au(HAL)NPs were injected into larvae that were then kept in three different conditions. As a control, a larva without any nanoparticles injected was also imaged. All larvae images are in the same orientation as the control larvae with the head (rostral) facing left and the tail (caudal) on the right.

3.5. Histological analysis

An interesting aspect also worth studying was the histological analysis of larvae injected with NPs. Stained sections of the injected larvae showed that most of the nanoparticles (easily distinguished due to the darkness in bright field optics over the HE staining) were mainly intermingled with lymphatic cells while digestive or Malpighian tubules appeared free of nanoparticles (Fig. 6). In contrast, PBS injected larvae showed no changes in the gross anatomical organ distribution as reported in other studies (Kristensen, 2003) (Fig. 6a). SeNPs showed the largest degree of accumulation leading to the biggest stellate-like aggregates that

17

337 were particularly abundant in the most caudal portions of the larvae (Fig. 6 b and c). These

338 aggregates largely differ from those observed after Ag- or Au(HAL)NPs injections that showed

339 smaller and dispersed aggregates along the rostrocaudal axis of the larvae (Fig. 6 d and e).

340 Additionally, SeNPs aggregates were often surrounded by large extracellular spaces and

341 numerous lymphoid cells were observed intermingled in these aggregates. However, in some
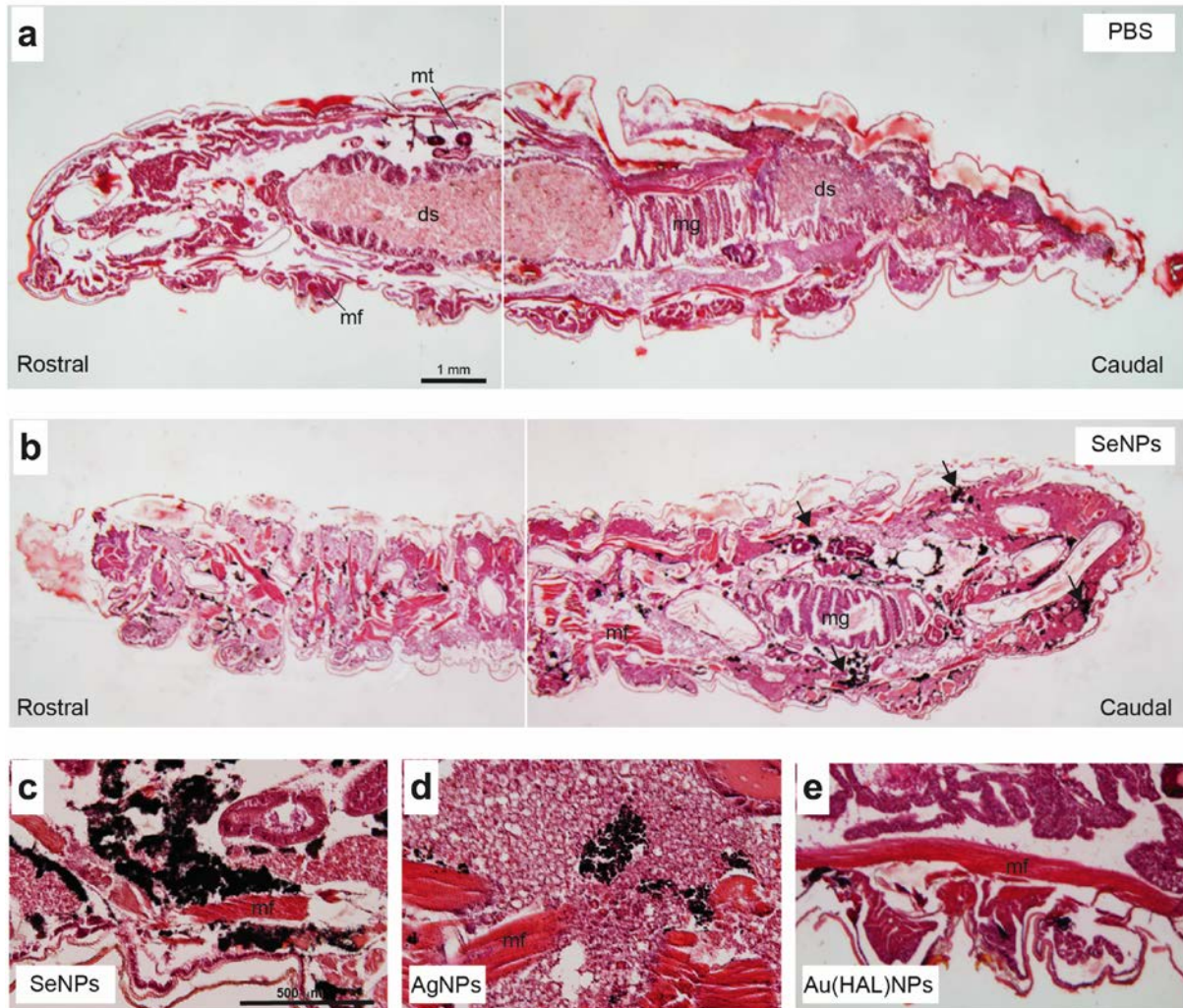
Fig. 6. Histological characterization of the distribution of Se, Ag, and Au(HAL) nanoparticles injected in *G. mellonella* larvae. **(a-b)** Examples of low power photomicrographs of *G. mellonella* larvae injected with **(a)** PBS and **(b)** SeNPs. The rostral and caudal portions of the larvae are indicated. Sections were processed for HE (see Materials and methods section for details). After staining, the digestive system (ds) with the transitional midgut/hindgut transition (mg), groups of muscle fascicles (mf) as well as the Malpighian tubules (mt) can be seen. Also, the intense dark labeling of the injected nanoparticles (i.e., SeNPs) can be seen (arrows in B). **(c-e)** High power photomicrographs illustrating examples of **(c)** Se, **(d)** Ag, and **(e)** Au(HAL) nanoparticle aggregates after injection. Notice the relevant size of the SeNPs aggregates compared to Ag or Au(HAL) NPs and the large extracellular spaces that surround the aggregates. Most aggregates are located in the lymphoid tissue and can be seen close to other larval structures like the mf or ds in some cases. Scale bars: A = 1 mm pertains to B; C = 500 mm pertains to D-E.

342 cases, NPs were close to striate muscle fascicles or Malpighi tubes. A similar situation, although

343 less relevant, was observed after AgNPs injection (Fig. 6d) and was not determined after

344 Au(HAL)NPs treatment (Fig. 6e).

3.6. Behavioral tracking studies

346   For behavioral studies, toxic concentrations of Au(HAL), Ag, and Se nanoparticles were

347 injected into *G. mellonella* larvae. One hour post-injection, the behavior of the larvae was

348 monitored for 73 seconds (Fig.7). The larvae with Au(HAL)NPs had behavioral patterns not

349 significantly different when compared to the control group. On the other hand, the larvae with

350 AgNPs and SeNPs yielded impaired movement with the latter ceasing movement entirely (Fig.

351 7a). This was further determined by also measuring the distance traveled by the larvae at the

352 same time point. The larvae with Au(HAL)NPs traveled 10.9 cm which is similar to the 12.4

353 cm traveled by the control larvae. On the other hand, the larvae with AgNPs and SeNPs had

354 significantly reduced motility (Fig. 7b). The larvae with AgNPs traveled 3.9 cm while the larvae

355 with SeNPs only moved 0.1 cm during the duration of the measurement.
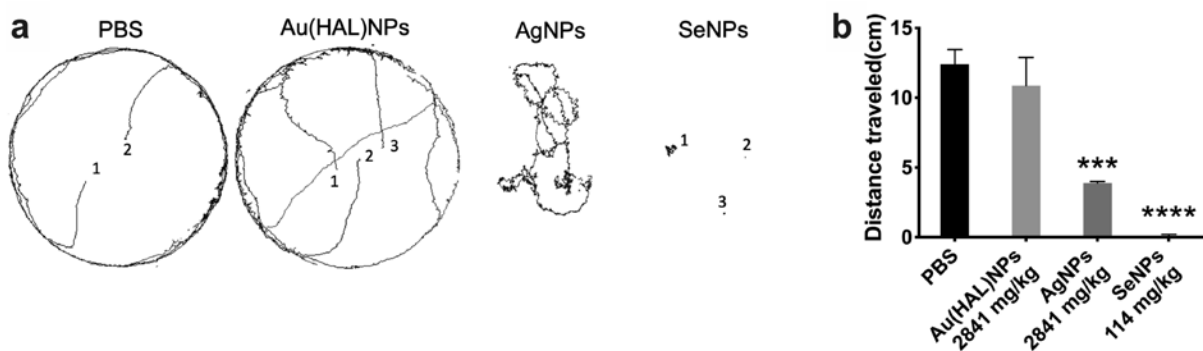
Fig. 7. Tracking of *G. mellonella* larvae movement after NPs injection. **(a)** Behavioral patterns of larvae injected with different concentrations of NPs and **(b)** distance traveled by larvae after NPs injection. Larvae were injected with PBS as a control. Asterisks: statistically significant difference versus PBS control in an unpaired *t*-test (***: *p*-value <0.001; ****: *p*-value <0.0001).

4. Discussion

357   As the use of nanoparticles is rapidly expanding, there is a critical need for efficient

358 assays to first determine the potential toxicity of NPs before their use in human applications.

359   Unlike toxicity studies *in vitro*, *in vivo* models tend to simulate the real conditions of the human

360   body more closely. Due to the ethical controversies surrounding murine models, it is currently

361   not possible to justify passing directly from nanomaterial synthesis to toxicity testing in rodents.

362   Therefore, toxicity screenings in non-rodent *in vivo* models are necessary as an intermediate

363   step. In this study, various types of nanoparticles were synthesized to evaluate the efficacy of

364   *G. mellonella* as *an in vivo* toxicological model.

365   The synthesis of Au(HAL)NPs, AgNPs, and SeNPs resulted in small yet stable spherical

366   particles which were found individually and for some of them, in aggregates. Small-sized

367   nanomaterials have a higher surface area that leads to a higher reactivity compared to their bulk

368   materials and this can be associated with possible toxic effects (Rabolli et al., 2011). Besides

369   size, the toxicity of NPs is also dependent on their shape, stability, agglomeration degree,

370   surface coating, functionalization, and purity (Luque-Garcia et al., 2013). Due to the increasing

371   applications of nanoparticles, numerous studies have been carried out to better understand their

372   toxicity. Here, the toxicity of different nanoparticles was tested both *in vitro* and *in vivo.*

373   Various concentrations of NPs were tested in A549 cells and in *G. mellonella* larvae to

374   determine their toxicity by defining the CC_{50} and LD_{50} of each type of nanoparticle. To see how

375   our *in vivo* model compared to already published data, LD_{50} values were gathered from

376   literature in which similar NPs were studied (Table 1). The A549 results were compared to data

377   obtained in macrophages to determine whether toxicity varies between cancerous epithelial

378   lung cells and macrophage cells. All types of nanoparticles tested were more toxic to

379   macrophages than to A549 cells. This could be due to the macrophages' ability to intake

380   nanoparticles more efficiently when compared to A549 cells (Kuhn et al., 2014). Cytotoxic

381   effects of NPs in culture media not only depend on the number of nanoparticles internalized by

382   cells but also on other factors such as incubation times, concentrations tested, and, clearly, the

383   type of cell lines used (Mukherjee et al., 2012; Luque-Garcia et al., 2013). Furthermore, the

20

same NPs can have inconsistent toxicity results when tested in different cell lines. In one study, the same dose of AuNPs was toxic to A549 cells but not to BHK21 and HepG2 cells (Patra et al., 2007). In another study, SeNPs inhibited the proliferation of A375, CNE2, HepG2, and MCF-7 cancer cells but were much less cytotoxic to normal Hs68 human fibroblasts (Chen et al., 2008). For these reasons, *in vitro* cytotoxicity assays are not the most optimal method to predict the toxicity of NPs as they are extremely dependent on the cell line used. Based on the literature, toxicity assays in murine models are oftentimes carried out by administering very few doses of nanoparticles to establish tissue accumulation and the levels of various hematological and biochemical markers. These assays are not done to determine LD_{50} values, most probably due to ethical and monetary motives. For this reason, it would be greatly advantageous to first define the LD_{50} doses in a model that screens a high number of samples and concentrations to reduce the number of NPs and mammals needed for testing. All of these conditions can be accomplished with the *G. mellonella in vivo* model. The LD_{50} values obtained with *G. mellonella* larvae are more similar to the values obtained with murine models when compared to *in vitro* models (Table 1). Therefore, *G. mellonella* shows to be a reliable and efficient non-rodent model for initial toxicity screenings of various nanoparticles over traditional cell assays.

To better understand the interactions between NPs and cells and other living organisms, it is important to determine whether NPs are taken up by cells and how they localize within cells and tissues. One study showed that NPs can quickly enter cells and disperse through the cytoplasm and nucleus which led to cytotoxicity that was more pronounced in the cells that had NPs within the nucleus (Lovrić et al., 2005). Another study revealed that NPs were found inside macrophages' lysosomes and mitochondria which was also related to higher cytotoxicity over time (Clift et al., 2011). These findings suggest that the intracellular fate of NPs could be directly linked to their toxicity. One of the proposed uptake mechanisms of NPs into cells is

21

409   endocytosis (Dobrovolskaia and McNeil, 2007; Kettler et al., 2014). This process is defined as

410   the uptake of extracellular material into eukaryotic cells by engulfing it with their cell

411   membrane. Several types of endocytosis exist, and the type employed by the cell depends on

412   the particle being internalized (Kuhn et al., 2014). Macrophages are known for their ability to

413   rapidly ingest and efficiently remove foreign particles (Juliano, 1988; Gustafson et al., 2015).

414   *In vitro* studies have shown that NPs are taken up by macrophages via phagocytosis and other

415   endocytosis pathways (Shukla et al., 2005; Krpetić et al., 2010; Kuhn et al., 2014). For this

416   reason, macrophages are a suitable cellular model to study the toxicity effects of NPs. Due to

417   the limitations of *in vitro* studies, the *G. mellonella* model offers a more valuable alternative.

418   *G. mellonella* larvae have an innate immune system, which consists of cellular and humoral

419   responses, that closely resembles the innate immune system in mammals. Cellular immune

420   responses are mediated by hemocytes and include phagocytosis, nodulation, and encapsulation

421   while humoral immune responses include melanization and synthesis of antimicrobial peptides.

422   Hemocytes present in the hemolymph of *G. mellonella* larvae are similar to macrophages found

423   in mammals. These cells can recognize foreign intruders by identifying humoral immune

424   effectors or through direct interaction of pathogen recognition proteins with pathogen-

425   associated molecular patterns (Cutuli et al., 2019).

426   The similarities between the cellular immune system of both *G. mellonella* and

427   mammals suggest that hemocyte density could be a good indicator of toxicity. Aneja et al.

428   demonstrated that triazole analogs were not toxic to *G. mellonella* larvae as seen by the lack of

429   hemocyte proliferation (Aneja et al., 2018). Maguire et al. administered potassium nitrate to *G.*

430   *mellonella* larvae and acute effects were evidenced by a significant increase in the number of

431   circulating hemocytes (Maguire et al., 2017). In this study, hemocyte density was quantified in

432   all groups of larvae injected with the different nanoparticles tested. As seen in Fig. 3, significant

433   hemocyte proliferation was seen in all of the concentrations and with all of the nanoparticles

434   tested. For both Au(HAL)NPs and AgNPs, the proliferation was highest with the lowest

435   concentrations tested while the proliferation decreased as the concentrations increased (Fig. 3

436   a and b). This could be due to hormesis which is characterized by stimulatory effects produced

437   by low doses of potentially toxic compounds (Stebbing, 1982). Jiao et al. found that non-

438   cytotoxic concentrations of AgNPs led to an accelerated proliferation of HepG2 cells due to

439   hormesis effects (Jiao et al., 2014). This acceleration was also seen with the lowest

440   concentration of Au(HAL)NPs tested in the present cytotoxicity studies. Therefore, hemocyte

441   proliferation could also be boosted by exposure of the larvae to low doses of AgNPs and

442   Au(HAL)NPs. In the case of functionalized AuNPs, the immunomodulatory effects seen could

443   be further explained by the surface functionalization. AuNPs functionalized with amino acids

444   are cationic, so they can be easily deposited by corona proteins and then recognized by

445   phagocytic or other clearing systems (Moyano et al., 2016). Another pattern seen with the

446   results was that as the concentrations of the Au(HAL) and Ag nanoparticles increased, the

447   hemocyte density decreased. This is most likely due to potential damage of hemopoietic organs

448   in the larvae due to NP toxicity (Eskin et al., 2019). For SeNPs, the hemocyte density remained

449   more or less constant throughout all of the concentrations tested (Fig. 3c). SeNPs were the most

450   toxic to the larvae so the absence of hemocyte proliferation could be due to increased cell death

451   as a result of the high toxicity.

452   To further demonstrate the similarities in the immune responses between *G. mellonella*

453   and mammals, NP internalization within cells was determined using confocal microscopy (Fig.

454   4). The obtained images clearly show that hemocytes were able to internalize Au(HAL) and Ag

455   nanoparticles. Although the exact mechanism of internalization cannot be determined by

456   confocal microscopy alone, it demonstrates that hemocytes are able to identify NPs as foreign

457   and thus trigger the larval immune response as it would occur in mammals. While hemocyte

458   proliferation is a clear indicator of an activated immune system, it is not a strong indicator of

23

459   the degree of toxicity being experienced by the larvae. This would be better determined by

460   combining hemocyte density measurements along with evaluating changes in hemocyte

461   morphology, proteomics, enzymatic activity, and histology, among others.

462   Nanoparticle distribution was also examined in the whole larvae. Microscopy images

463   revealed that the NPs were located in the caudal part of the larvae with the majority of the NPs

464   accumulating at the tails (Figs. 5 and 6). This event was still seen when the movement of the

465   larvae was partially or fully restricted (Fig. 5b) thus suggesting that the NP accumulation is not

466   due to the peristaltic motility movement of the worm. Although the movement was limited,

467   NPs could still possibly move through the hemolymph due to contractions of the larval

468   abdominal spiracles during respiration (Wasserthal, 1996). Another unknown mechanism could

469   be further responsible for the accumulation of large quantities of NPs in the caudal part of the

470   larvae, but more studies are needed to better understand this phenomenon. Histological findings

471   confirmed that the NPs were found in aggregates in the most caudal part of the larvae (Fig. 6).

472   In terms of aggregates and the appearance of extracellular spaces, it seems that the presence (in

473   the case of SeNPs) of i) an enlarged accumulation of lymphoid/hemocytes cells after SeNPs

474   injection compared to AgNPs and Au(HAL)NPs or ii) increased cell death is due to toxic

475   activity. AgNPs were observed in the same locations as the SeNPs; however, the size of the

476   aggregates is smaller and the size of the extracellular space around these aggregates is also

477   smaller. Thus, cell or larval death could be observed at higher survival times as it occurred with

478   the LD_{50} experiments. This could also be the case for the AgNPs that were only present in the

479   hemolymph. As the larvae were killed 1-hour post-injection, more time might be needed to see

480   tissue damage like the one seen with SeNPs. Regardless, 1 hour was enough for the larvae to

481   undergo a faster color change after injection with SeNPs compared to the other NPs. A

482   drawback of HE is that dying cells cannot be fully characterized and only gross anatomical

483   changes can be clearly ascertained. For this reason, histological findings should be combined

484 with other studies. In this case, the histological results corroborate the results obtained with the

485 hemocyte density experiments as well as the microscopy studies.

486   Finally, another way to study the toxicity of NPs in *G. mellonella* is to examine the

487 behavior of the larvae after NP inoculation. Changes in movement and behavior were seen in

488 *Drosophila melanogaster* and *Danio rerio*, respectively, after exposure to AgNPs (Armstrong

489 et al., 2013; Krishnaraj et al., 2016). The NPs in both studies were administered through feeding

490 which does not truly mimic the typical administration route for drug delivery. In contrast, the

491 injection of NPs into *G. mellonella* larvae can be easily accomplished. In this study, the

492 behavior of larvae injected with toxic concentrations of NPs was assessed (Fig. 7). The larvae

493 injected with Au(HAL)NPs maintained a normal behavior similar to the larvae injected with

494 PBS. This result was expected as this NP concentration was lethal to the larvae after several

495 hours post-injection. On the other hand, the toxicity of AgNPs and SeNPs was soon witnessed

496 by the color changes of the larvae from cream to dark accompanied with significantly reduced

497 motility. SeNPs were the most toxic to the larvae as evidenced by the complete lack of

498 movement soon after injection. These results further validate the toxicity effects observed with

499 all of the experiments mentioned above.

500   The consistency in all of the results obtained with the different experiments performed

501 to study NP toxicity using *G. mellonella* demonstrates the significant utility of this animal

502 model. With this alternative model, toxicity screenings of various NPs can be performed

503 economically and conveniently, and the results obtained will be more reliable than traditional

504 *in vitro* models without any ethical limitations. *G. mellonella* can be used as a bridge between

505 cytotoxicity and *in vivo* murine assays, thus allowing for more accurate predictions of the

506 toxicity effects brought upon by nanoparticles.

507

521

Declaration of interests

523   The authors declare no conflicts of interest.

524

525

526 **References**

527 Ahamed, M., Alsalhi, M.S., Siddiqui, M.K., 2010. Silver nanoparticle applications and human

528   health. Clin Chim Acta 411, 1841-1848.

529 Alkilany, A.M., Murphy, C.J., 2010. Toxicity and cellular uptake of gold nanoparticles: what

530   we have learned so far? J Nanopart Res 12, 2313-2333.

531 Allegra, E., Titball, R.W., Carter, J., Champion, O.L., 2018. *Galleria mellonella* larvae allow

532   the discrimination of toxic and non-toxic chemicals. Chemosphere 198, 469-472.

533 Aneja, B., Azam, M., Alam, S., Perwez, A., Maguire, R., Yadava, U., Kavanagh, K., Daniliuc,

534   C.G., Rizvi, M.M.A., Haq, Q.M.R., Abid, M., 2018. Natural Product-Based 1,2,3-

535   Triazole/Sulfonate Analogues as Potential Chemotherapeutic Agents for Bacterial

536   Infections. ACS Omega 3, 6912-6930.

537 Arai, Y., Miyayama, T., Hirano, S., 2015. Difference in the toxicity mechanism between ion

538   and nanoparticle forms of silver in the mouse lung and in macrophages. Toxicology

539   328, 84-92.

540 Armstrong, N., Ramamoorthy, M., Lyon, D., Jones, K., Duttaroy, A., 2013. Mechanism of

541   silver nanoparticles action on insect pigmentation reveals intervention of copper

542   homeostasis. PLoS One 8, e53186.

543 Barile, F.A., 2013. Principles of Toxicology Testing, 2 ed. CRC Press, Boca Raton.

544 Bouwmeester, H., Brandhoff, P., Marvin, H.J.P., Weigel, S., Peters, R.J.B., 2014. State of the

545   safety assessment and current use of nanomaterials in food and food production. Trends

546   in Food Science and Technology 40, 200-210.

547 Bronzetti, G., Cini, M., Andreoli, E., Caltavuturo, L., Panunzio, M., Croce, C.D., 2001.

548   Protective effects of vitamins and selenium compounds in yeast. Mutat Res 496, 105-

549   115.

550 Browne, N., Heelan, M., Kavanagh, K., 2013. An analysis of the structural and functional

551   similarities of insect hemocytes and mammalian phagocytes. Virulence 4, 597-603.

552 Chairuangkitti, P., Lawanprasert, S., Roytrakul, S., Aueviriyavit, S., Phummiratch, D.,

553   Kulthong, K., Chanvorachote, P., Maniratanachote, R., 2013. Silver nanoparticles

554   induce toxicity in A549 cells via ROS-dependent and ROS-independent pathways.

555   Toxicol In Vitro 27, 330-338.

556 Champion, O.L., Wagley, S., Titball, R.W., 2016. *Galleria mellonella* as a model host for

557   microbiological and toxin research. Virulence 7, 840-845.

558 Chen, T., Wong, Y.S., Zheng, W., Bai, Y., Huang, L., 2008. Selenium nanoparticles fabricated

559   in *Undaria pinnatifida* polysaccharide solutions induce mitochondria-mediated

560   apoptosis in A375 human melanoma cells. Colloids Surf B Biointerfaces 67, 26-31.

561 Chen, Y.S., Hung, Y.C., Liau, I., Huang, G.S., 2009. Assessment of the In Vivo Toxicity of

562   Gold Nanoparticles. Nanoscale Res Lett 4, 858-864.

563 Clift, M.J., Brandenberger, C., Rothen-Rutishauser, B., Brown, D.M., Stone, V., 2011. The

564   uptake and intracellular fate of a series of different surface coated quantum dots in vitro.

565   Toxicology 286, 58-68.

566 Cutuli, M.A., Petronio Petronio, G., Vergalito, F., Magnifico, I., Pietrangelo, L., Venditti, N.,

567   Di Marco, R., 2019. *Galleria mellonella* as a consolidated in vivo model hosts: New

568   developments in antibacterial strategies and novel drug testing. Virulence 10, 527-541.

569 De Jong, W.H., Hagens, W.I., Krystek, P., Burger, M.C., Sips, A.J., Geertsma, R.E., 2008.

570   Particle size-dependent organ distribution of gold nanoparticles after intravenous

571   administration. Biomaterials 29, 1912-1919.

572 De Jong, W.H., Van Der Ven, L.T., Sleijffers, A., Park, M.V., Jansen, E.H., Van Loveren, H.,

573   Vandebriel, R.J., 2013. Systemic and immunotoxicity of silver nanoparticles in an

574   intravenous 28 days repeated dose toxicity study in rats. Biomaterials 34, 8333-8343.

575   Desbois, A.P., Coote, P.J., 2012. Utility of Greater Wax Moth Larva (*Galleria mellonella*) for

576   Evaluating the Toxicity and Efficacy of New Antimicrobial Agents. Adv Appl

577   Microbiol 78, 25-53.

578   Dobrovolskaia, M.A., McNeil, S.E., 2007. Immunological properties of engineered

579   nanomaterials. Nat Nanotechnol 2, 469-478.

580   Dolan, N., Gavin, D.P., Eshwika, A., Kavanagh, K., McGinley, J., Stephens, J.C., 2016.

581   Synthesis, antibacterial and anti-MRSA activity, in vivo toxicity and a structure-activity

582   relationship study of a quinoline thiourea. Bioorg Med Chem Lett 26, 630-635.

583   Eskin, A., Öztürk, Ş., Körükçü, M., 2019. Determination of the acute toxic effects of zinc oxide

584   nanoparticles (ZnO NPs) in total hemocytes counts of *Galleria mellonella* (Lepidoptera:

585   Pyralidae) with two different methods. Ecotoxicology 28, 801-808.

586   Evans, S.O., Khairuddin, P.F., Jameson, M.B., 2017. Optimising Selenium for Modulation of

587   Cancer Treatments. Anticancer Res 37, 6497-6509.

588   Fernandes, A.P., Gandin, V., 2015. Selenium compounds as therapeutic agents in cancer.

589   Biochim Biophys Acta 1850, 1642-1660.

590   Finkelstein, A.E., Walz, D.T., Batista, V., Mizraji, M., Roisman, F., Misher, A., 1976.

591   Auranofin. New oral gold compound for treatment of rheumatoid arthritis. Ann Rheum

592   Dis 35, 251-257.

593   Gangadoo, S., Dinev, I., Willson, N.L., Moore, R.J., Chapman, J., Stanley, D., 2020.

594   Nanoparticles of selenium as high bioavailable and non-toxic supplement alternatives

595   for broiler chickens. Environ Sci Pollut Res Int.

596   Goodman, C.M., McCusker, C.D., Yilmaz, T., Rotello, V.M., 2004. Toxicity of gold

597   nanoparticles functionalized with cationic and anionic side chains. Bioconjug Chem 15,

598   897-900.

599   Gustafson, H.H., Holt-Casper, D., Grainger, D.W., Ghandehari, H., 2015. Nanoparticle Uptake:

600   The Phagocyte Problem. Nano Today 10, 487-510.

601   Hashimoto, M., Sasaki, J.I., Yamaguchi, S., Kawai, K., Kawakami, H., Iwasaki, Y., Imazato,

602   S., 2015. Gold Nanoparticles Inhibit Matrix Metalloproteases without Cytotoxicity. J

603   Dent Res 94, 1085-1091.

604   Hsin, Y.H., Chen, C.F., Huang, S., Shih, T.S., Lai, P.S., Chueh, P.J., 2008. The apoptotic effect

605   of nanosilver is mediated by a ROS- and JNK-dependent mechanism involving the

606   mitochondrial pathway in NIH3T3 cells. Toxicol Lett 179, 130-139.

607   Ignasiak, K., Maxwell, A., 2017. *Galleria mellonella* (greater wax moth) larvae as a model for

608   antibiotic susceptibility testing and acute toxicity trials. BMC Res Notes 10, 428.

609   Jevtić, M., Mitrić, M., Škapin, S., Jančar, B., Ignjatović, N., Uskoković, D., 2008. Crystal

610   Structure of Hydroxyapatite Nanorods Synthesized by Sonochemical Homogeneous

611   Precipitation. Crystal Growth & Design 8, 2217-2222.

612   Jia, H.Y., Liu, Y., Zhang, X.J., Han, L., Du, L.B., Tian, Q., Xu, Y.C., 2009. Potential oxidative

613   stress of gold nanoparticles by induced-NO releasing in serum. J Am Chem Soc 131,

614   40-41.

615   Jiao, Z.H., Li, M., Feng, Y.X., Shi, J.C., Zhang, J., Shao, B., 2014. Hormesis effects of silver

616   nanoparticles at non-cytotoxic doses to human hepatoma cells. PLoS One 9, e102564.

617   Jones, C.F., Grainger, D.W., 2009. In vitro assessments of nanomaterial toxicity. Adv Drug

618   Deliv Rev 61, 438-456.

619   Juliano, R.L., 1988. Factors affecting the clearance kinetics and tissue distribution of liposomes,

620   microspheres and emulsions. Advanced Drug Delivery Reviews 2, 31-54.

621   Junqueira, J.C., 2012. *Galleria mellonella* as a model host for human pathogens: recent studies

622   and new perspectives. Virulence 3, 474-476.

623   Kettler, K., Veltman, K., van de Meent, D., van Wezel, A., Hendriks, A.J., 2014. Cellular

624   uptake of nanoparticles as determined by particle properties, experimental conditions,

625   and cell type. Environ Toxicol Chem 33, 481-492.

626   Khoshnevisan, K., Daneshpour, M., Barkhi, M., Gholami, M., Samadian, H., Maleki, H., 2018.

627   The promising potentials of capped gold nanoparticles for drug delivery systems. J Drug

628   Target 26, 525-532.

629   Kim, J.H., Kim, K.W., Kim, M.H., Yu, Y.S., 2009a. Intravenously administered gold

630   nanoparticles pass through the blood-retinal barrier depending on the particle size, and

631   induce no retinal toxicity. Nanotechnology 20, 505101.

632   Kim, S., Choi, J.E., Choi, J., Chung, K.H., Park, K., Yi, J., Ryu, D.Y., 2009b. Oxidative stress-

633   dependent toxicity of silver nanoparticles in human hepatoma cells. Toxicol In Vitro

634   23, 1076-1084.

635   Kim, Y.S., Song, M.Y., Park, J.D., Song, K.S., Ryu, H.R., Chung, Y.H., Chang, H.K., Lee,

636   J.H., Oh, K.H., Kelman, B.J., Hwang, I.K., Yu, I.J., 2010. Subchronic oral toxicity of

637   silver nanoparticles. Part Fibre Toxicol 7, 20.

638   Krishnaraj, C., Harper, S.L., Yun, S.I., 2016. In Vivo toxicological assessment of biologically

639   synthesized silver nanoparticles in adult Zebrafish (*Danio rerio*). J Hazard Mater 301,

640   480-491.

641   Kristensen, N., 2003. Arthropoda: Insecta. in: Kristensen, N. (Ed.). Lepidoptera: Moths and

642   Butterflies. Handbuch der Zoologie Volume 4. De Gruyter.

643   Krpetić, Z., Porta, F., Caneva, E., Dal Santo, V., Scarì, G., 2010. Phagocytosis of biocompatible

644   gold nanoparticles. Langmuir 26, 14799-14805.

645   Kuhn, D.A., Vanhecke, D., Michen, B., Blank, F., Gehr, P., Petri-Fink, A., Rothen-Rutishauser,

646   B., 2014. Different endocytotic uptake mechanisms for nanoparticles in epithelial cells

647   and macrophages. Beilstein J Nanotechnol 5, 1625-1636.

648 Letavayova, L., Vlasakova, D., Spallholz, J.E., Brozmanova, J., Chovanec, M., 2008. Toxicity

649   and mutagenicity of selenium compounds in *Saccharomyces cerevisiae*. Mutat Res 638,

650   1-10.

651 Leung, M.C., Williams, P.L., Benedetto, A., Au, C., Helmcke, K.J., Aschner, M., Meyer, J.N.,

652   2008. *Caenorhabditis elegans*: an emerging model in biomedical and environmental

653   toxicology. Toxicol Sci 106, 5-28.

654 Lovrić, J., Bazzi, H.S., Cuie, Y., Fortin, G.R., Winnik, F.M., Maysinger, D., 2005. Differences

655   in subcellular distribution and toxicity of green and red emitting CdTe quantum dots. J

656   Mol Med (Berl) 83, 377-385.

657 Luque-Garcia, J.L., Sanchez-Díaz, R., Lopez-Heras, I., Martin, P., Camara, C., 2013.

658   Bioanalytical strategies for *in-vitro* and *in-vivo* evaluation of the toxicity induced by

659   metallic nanoparticles. Trends in Analytical Chemistry 43, 254-268.

660 Maguire, R., Duggan, O., Kavanagh, K., 2016. Evaluation of *Galleria mellonella* larvae as an

661   in vivo model for assessing the relative toxicity of food preservative agents. Cell Biol

662   Toxicol 32, 209-216.

663 Maguire, R., Kunc, M., Hyrsl, P., Kavanagh, K., 2017. Analysis of the acute response of

664   *Galleria mellonella* larvae to potassium nitrate. Comp Biochem Physiol C Toxicol

665   Pharmacol 195, 44-51.

666 Makama, S., Kloet, S.K., Piella, J., van den Berg, H., de Ruijter, N.C.A., Puntes, V.F., Rietjens,

667   I.M.C.M., van den Brink, N.W., 2018. Effects of Systematic Variation in Size and

668   Surface Coating of Silver Nanoparticles on Their In Vitro Toxicity to Macrophage

669   RAW 264.7 Cells. Toxicol Sci 162, 79-88.

670 Mannerström, M., Zou, J., Toimela, T., Pyykkö, I., Heinonen, T., 2016. The applicability of

671   conventional cytotoxicity assays to predict safety/toxicity of mesoporous silica

672 nanoparticles, silver and gold nanoparticles and multi-walled carbon nanotubes. Toxicol

673 In Vitro 37, 113-120.

674 Megaw, J., Thompson, T.P., Lafferty, R.A., Gilmore, B.F., 2015. *Galleria mellonella* as a novel

675 in vivo model for assessment of the toxicity of 1-alkyl-3-methylimidazolium chloride

676 ionic liquids. Chemosphere 139, 197-201.

677 Mijnendonckx, K., Leys, N., Mahillon, J., Silver, S., Van Houdt, R., 2013. Antimicrobial silver:

678 uses, toxicity and potential for resistance. Biometals 26, 609-621.

679 Moya-Anderico, L., Admella, J., Torrents, E., 2020. A clearing protocol for *Galleria mellonella*

680 larvae: Visualization of internalized fluorescent nanoparticles. N Biotechnol.

681 Moyano, D.F., Liu, Y., Ayaz, F., Hou, S., Puangploy, P., Duncan, B., Osborne, B.A., Rotello,

682 V.M., 2016. Immunomodulatory effects of coated gold nanoparticles in LPS-stimulated.

683 Chem 1, 320-327.

684 Mukherjee, S.G., O'Claonadh, N., Casey, A., Chambers, G., 2012. Comparative in vitro

685 cytotoxicity study of silver nanoparticle on two mammalian cell lines. Toxicol In Vitro

686 26, 238-251.

687 Patra, H.K., Banerjee, S., Chaudhuri, U., Lahiri, P., Dasgupta, A.K., 2007. Cell selective

688 response to gold nanoparticles. Nanomedicine 3, 111-119.

689 Pinzaru, I., Coricovac, D., Dehelean, C., Moacă, E.A., Mioc, M., Baderca, F., Sizemore, I.,

690 Brittle, S., Marti, D., Calina, C.D., Tsatsakis, A.M., Șoica, C., 2018. Stable PEG-coated

691 silver nanoparticles - A comprehensive toxicological profile. Food Chem Toxicol 111,

692 546-556.

693 Pratsinis, A., Hervella, P., Leroux, J.C., Pratsinis, S.E., Sotiriou, G.A., 2013. Toxicity of silver

694 nanoparticles in macrophages. Small 9, 2576-2584.

695   Rabolli, V., Thomassen, L.C., Uwambayinema, F., Martens, J.A., Lison, D., 2011. The

696   cytotoxic activity of amorphous silica nanoparticles is mainly influenced by surface area

697   and not by aggregation. Toxicol Lett 206, 197-203.

698   Ramarao, N., Nielsen-Leroux, C., Lereclus, D., 2012. The insect *Galleria mellonella* as a

699   powerful infection model to investigate bacterial pathogenesis. J Vis Exp, e4392.

700   Rand, M.D., Montgomery, S.L., Prince, L., Vorojeikina, D., 2014. Developmental toxicity

701   assays using the *Drosophila* model. Curr Protoc Toxicol 59, 1 12 11-20.

702   Rayman, M.P., 2012. Selenium and human health. Lancet 379, 1256-1268.

703   Recordati, C., De Maglie, M., Bianchessi, S., Argentiere, S., Cella, C., Mattiello, S., Cubadda,

704   F., Aureli, F., D'Amato, M., Raggi, A., Lenardi, C., Milani, P., Scanziani, E., 2016.

705   Tissue distribution and acute toxicity of silver after single intravenous administration in

706   mice: nano-specific and size-dependent effects. Part Fibre Toxicol 13, 12.

707   Ren, S.X., Zhan, B., Lin, Y., Ma, D.S., Yan, H., 2019. Selenium Nanoparticles Dispersed in

708   Phytochemical Exert Anti-Inflammatory Activity by Modulating Catalase, GPx1, and

709   COX-2 Gene Expression in a Rheumatoid Arthritis Rat Model. Med Sci Monit 25, 991-

710   1000.

711   Rinna, A., Magdolenova, Z., Hudecova, A., Kruszewski, M., Refsnes, M., Dusinska, M., 2015.

712   Effect of silver nanoparticles on mitogen-activated protein kinases activation: role of

713   reactive oxygen species and implication in DNA damage. Mutagenesis 30, 59-66.

714   Rohn, I., Marschall, T.A., Kroepfl, N., Jensen, K.B., Aschner, M., Tuck, S., Kuehnelt, D.,

715   Schwerdtle, T., Bornhorst, J., 2018. Selenium species-dependent toxicity,

716   bioavailability and metabolic transformations in *Caenorhabditis elegans*. Metallomics

717   10, 818-827.

718   Schluesener, J.K., Schluesener, H.J., 2013. Nanosilver: application and novel aspects of

719   toxicology. Arch Toxicol 87, 569-576.

720   Shahabi, R., Anissian, A., Javadmoosavi, S.A., Nasirinezhad, F., 2019. Protective and anti-

721   inflammatory effect of selenium nano-particles against bleomycin-induced pulmonary

722   injury in male rats. Drug Chem Toxicol, 1-9.

723   Shrivastava, R., Kushwaha, P., Bhutia, Y.C., Flora, S., 2016. Oxidative stress following

724   exposure to silver and gold nanoparticles in mice. Toxicol Ind Health 32, 1391-1404.

725   Shukla, R., Bansal, V., Chaudhary, M., Basu, A., Bhonde, R.R., Sastry, M., 2005.

726   Biocompatibility of gold nanoparticles and their endocytotic fate inside the cellular

727   compartment: a microscopic overview. Langmuir 21, 10644-10654.

728   Sonavane, G., Tomoda, K., Makino, K., 2008. Biodistribution of colloidal gold nanoparticles

729   after intravenous administration: effect of particle size. Colloids Surf B Biointerfaces

730   66, 274-280.

731   Souza, T.A., Franchi, L.P., Rosa, L.R., da Veiga, M.A., Takahashi, C.S., 2016. Cytotoxicity

732   and genotoxicity of silver nanoparticles of different sizes in CHO-K1 and CHO-XRS5

733   cell lines. Mutat Res Genet Toxicol Environ Mutagen 795, 70-83.

734   Stebbing, A.R., 1982. Hormesis--the stimulation of growth by low levels of inhibitors. Sci Total

735   Environ 22, 213-234.

736   Tang, J., Xiong, L., Wang, S., Wang, J., Liu, L., Li, J., Yuan, F., Xi, T., 2009. Distribution,

737   translocation and accumulation of silver nanoparticles in rats. J Nanosci Nanotechnol

738   9, 4924-4932.

739   Thomas, R.J., Hamblin, K.A., Armstrong, S.J., Muller, C.M., Bokori-Brown, M., Goldman, S.,

740   Atkins, H.S., Titball, R.W., 2013. *Galleria mellonella* as a model system to test the

741   pharmacokinetics and efficacy of antibiotics against *Burkholderia pseudomallei*. Int J

742   Antimicrob Agents 41, 330-336.

743   Valdiglesias, V., Pasaro, E., Mendez, J., Laffon, B., 2010. In vitro evaluation of selenium

744   genotoxic, cytotoxic, and protective effects: a review. Arch Toxicol 84, 337-351.

745   Vance, M.E., Kuiken, T., Vejerano, E.P., McGinnis, S.P., Hochella, M.F., Jr., Rejeski, D., Hull,

746   M.S., 2015. Nanotechnology in the real world: Redeveloping the nanomaterial

747   consumer products inventory. Beilstein J Nanotechnol 6, 1769-1780.

748   Vukomanović, M., Logar, M., Škapin, S.D., Suvorov, D., 2014. Hydroxyapatite/gold/arginine:

749   designing the structure to create antibacterial activity. J Mater Chem B 2, 1557-1564.

750   Wasserthal, L.T., 1996. Interaction of Circulation and Tracheal Ventilation in Holometabolous

751   Insects. in: Evans, P.D. (Ed.). Advances in Insect Physiology. Academic Press, pp. 297-

752   351.

753   Wojda, I., 2017. Immunity of the greater wax moth *Galleria mellonella*. Insect Sci 24, 342-

754   357.

755   Xue, Y., Zhang, S., Huang, Y., Zhang, T., Liu, X., Hu, Y., Zhang, Z., Tang, M., 2012. Acute

756   toxic effects and gender-related biokinetics of silver nanoparticles following an

757   intravenous injection in mice. J Appl Toxicol 32, 890-899.

758   Yan, L., Spallholz, J.E., 1993. Generation of reactive oxygen species from the reaction of

759   selenium compounds with thiols and mammary tumor cells. Biochem Pharmacol 45,

760   429-437.

761   Yazhiniprabha, M., Vaseeharan, B., 2019. In vitro and in vivo toxicity assessment of selenium

762   nanoparticles with significant larvicidal and bacteriostatic properties. Mater Sci Eng C

763   Mater Biol Appl 103, 109763.

764   Zhang, Q., Hitchins, V.M., Schrand, A.M., Hussain, S.M., Goering, P.L., 2011. Uptake of gold

765   nanoparticles in murine macrophage cells without cytotoxicity or production of pro-

766   inflammatory mediators. Nanotoxicology 5, 284-295.

767   Zhang, X.D., Wu, H.Y., Wu, D., Wang, Y.Y., Chang, J.H., Zhai, Z.B., Meng, A.M., Liu, P.X.,

768   Zhang, L.A., Fan, F.Y., 2010. Toxicologic effects of gold nanoparticles in vivo by

769   different administration routes. Int J Nanomedicine 5, 771-781.

770   Zhang, Y., Ferguson, S.A., Watanabe, F., Jones, Y., Xu, Y., Biris, A.S., Hussain, S., Ali, S.F.,

771   2013. Silver nanoparticles decrease body weight and locomotor activity in adult male

772   rats. Small 9, 1715-1720.

773